Model Discrimination for Multicomponent Distillation – A Geometrical Approach for Total Reflux

Thomas Waltermann[1], Stefan Schlueter[1], Regina Benfer[2], Carsten Knoesche[2], Andrzej Górak[1,3], and Mirko Skiborowski[1,*]

DOI: 10.1002/cite.202000026

While rate-based models are available in commercial flowsheet simulation tools, packed distillation columns are still mostly designed based on the equilibrium stage model in combination with HETP values. In order to discriminate between both types of models in a simple way, this article proposes an algorithmic test, based on a geometric criterion for total reflux operation. Substantial differences are illustrated especially for wide-boiling mixtures, while component-specific mass transfer rates either increase or reduce the deviation. The derived results are validated by dedicated experiments.

Keywords: Distillation, Equilibrium stage model, Model discrimination, Rate-based model

Received: March 05, 2020; *revised:* May 01, 2020; *accepted:* May 07, 2020

1 Introduction

Distillation remains the most applied process for the separation of liquid mixtures and product purification in the chemical industry. Distillation processes are usually conducted in columns equipped with either trays or packings, while different mathematical models are used for the design of these columns. Various textbooks present detailed descriptions of the different internals, decision criteria for a specific type of internal and related operational constraints, as well as the relevant modeling approaches [1–5]. Despite the rich history in distillation related research [6], the state-of-the-art approach for the design of distillation columns in industry remains a sequential procedure, in which first the required separation effort is determined based on thermodynamic calculations using the equilibrium stage (EQ) model [7]. Based on the EQ model, which dates back to Sorel's work in the 19th century [8], the necessary number of equilibrium stages and energy requirements for a specific separation are determined. For this purpose, a coupled algebraic equation system that accounts for mass and enthalpy balances, summation constraints and equilibrium conditions, the so-called MESH equations [9], needs to be solved. The actual height of a packed column is further determined based on a value that describes the height equivalent to a theoretical plate (HETP), which is specific for the selected internal and is usually determined experimentally for binary test mixtures, while experiments with the real system may be necessary in case of strongly non-ideal systems, including most aqueous systems [10]. This combination of a MESH-based model and HETP values was established more than 80 years ago by Chilton and Colburn [11]. Although this design approach is computationally efficient, the resulting column design can be inappropriate for certain separation tasks. By application to other chemical systems and especially multicomponent mixtures, it is implicitly assumed that the HETP values depend only on the *F*-factor and the operating pressure. The potential limitation of this assumption has, e.g., been illustrated for columns equipped with random packings by Górak et al. [12]. In general, it has to be assumed that the HETP value is affected by the hydrodynamics and the transport properties of the processed chemical system and, thus, also varies along the column height [9]. Therefore, it is common practice to adjust the HETP values based on available data for similar chemical systems or dedicated experiments. Especially for multicomponent systems these variations may, however, become significant and HETP values may not suffice to account for variations in component-specific mass transfer rates [9].

[1]Thomas Waltermann, Stefan Schlueter, Prof. Dr.-Ing. Andrzej Górak, Prof. Dr.-Ing. Mirko Skiborowski
mirko.skiborowski@tu-dortmund.de
TU Dortmund University, Department of Biochemical and Chemical Engineering, Laboratory of Fluid Separations, Emil-Figge-Straße 70, 44227 Dortmund, Germany.

[2]Dr. Regina Benfer, Dr. Carsten Knoesche
BASF SE, GCP/TA – L540, 67056 Ludwigshafen am Rhein, Germany.

[3]Prof. Dr.-Ing. Andrzej Górak
Lodz University of Technology, Faculty of Process and Environmental Engineering, Department of Environmental Engineering, Wólczańska 213, 90-924 Lódz, Poland.

In order to overcome the limitations of the EQ-based design approach, physically more profound non-equilibrium modeling and design approaches were developed, which according to Górak [13] and Kenig [14] build either on rate-based (RB) models that account for transfer phenomena in a reduced way, mostly assuming 1D plug flow along the column height, or physically more profound computational fluid dynamic (CFD) models, which try to describe transport phenomena in a geometrically resolved fashion. While the latter approach is the most rigorous, it has not yet been applied to the design of full distillation columns, due to the complex multiphase fluid dynamics and the unknown localization of the phase boundaries within the column [14]. To build a bridge between the detailed and complex flow patterns in real separation columns equipped with structured packings and (a combination of) geometrically simpler flows, Kenig [15] and Kenig and Shilkin [16] proposed the so-called hydrodynamic analogy (HDA) approach, which enables the description of the fluid dynamics in a column with high accuracy. While CFD and HDA have not been applied to the design of whole distillation columns, they can effectively complement the design and optimization of distillation columns on the micro- and mesoscale when combined in a complementary approach with the macroscale model of the column represented by either EQ or RB models [17].

An approach based on differential mass and energy balances for the liquid and vapor phases that accounts for heat and mass transfer rates between both phases, building on the two film theory [18, 19], while assuming 1D plug flow behavior, is the most applied RB modeling and design approach. The 1D plug flow assumption can be relaxed, by using so-called cell models, which divide stages along the column height into a number of parallel contacting cells, in order to account for potential maldistribution in horizontal direction, evaluating flow patterns by means of a cell flow model [9, 20, 21]. Despite this possible extension we will, however, limit the subsequent discussion to the 1D plug flow assumption, when referring to the RB model. In any way, the RB model is more complex than the EQ model and requires equipment-specific correlations as well as knowledge about additional physical transport properties [9, 14]. The RB model can either be formulated as a differential algebraic equation system, as described by Serwinski and Górak [19], or as a finite difference model, as described by Krishnamurthy and Taylor [18]. Unlike the MESH equations for the EQ model, the RB model is based on the so-called MERSHQ equations, which also account for *m*ass and *e*nergy balances, as well as *s*ummation and e*q*uilibrium equations, but furthermore include mass and heat transfer *r*ate equations and *h*ydraulic equations that depict the pressure drop. The finite difference model is the more common model, which is also available in flowsheet simulation software, such as Aspen Plus® or ChemSep. While the physical property and model requirements are considerably larger for the RB model compared to the EQ model, Taylor and Krishna [5] already pointed out that the necessary equations for mass transfer have been known for at least as long as the EQ model. The additional effort in setting up and solving the RB model was, however, frequently reported as of high value, providing much more accurate representations of experimental results [9, 12, 22, 23]. It is also worth pointing out that especially the differences in the requirements for physical properties diminish largely, in case the HETP values are computed from correlations of the mass transfer coefficients [3].

Accounting for the benefits of both models, Taylor et al. [9] suggest to further utilize EQ models in the conceptual design phase, exploiting different column configurations and process designs, but finally checking the resulting column designs against the RB model, in order to avoid inappropriate column designs. This is in line with other suggestions on model-based design of distillation columns [1, 10]. While this solution is certainly feasible, it would be beneficial to determine the need to apply the RB model as early as possible. Unfortunately, to this point, no heuristics or simple calculation methods have been proposed to answer this question for a specific separation task. With the current publication we want to start to fill this gap, by introducing a simplified geometrical method, which checks in how far the composition trajectories obtained by the solution of the EQ and RB model deviate from each other, independent of the choice of HETP values, considering the limiting case of total reflux.

The main reasoning for choosing the composition trajectories as the basis for the model discrimination is further described in the next section, which also provides a review of the related preceding work of other authors. After this more detailed motivation, Sect. 3 describes the calculation procedures for the EQ and RB composition trajectories and introduces the maximum value of the shortest Euclidean distances between the different composition profiles as the discrimination criterion. Subsequently, in Sect. 4 the presented methodology is applied in a sensitivity analysis with one-at-a-time variations to analyze the influence of the VLE and component-specific mass transfer rates on the differences between the EQ and RB composition trajectories. Based on this sensitivity analysis real multicomponent mixtures are selected for further simulations, before Sect. 5 illustrates a validation of the results by dedicated experimental investigations. Finally, Sect. 6 provides a brief summary and conclusion of the conducted studies as well as an outlook on future work for the extension towards design calculations at finite reflux.

2 State of the Art

As indicated in the introduction, the comparison of the composition trajectories calculated from the RB and EQ models is deemed as an effective means for model discrimination. In this context, a composition trajectory represents

the liquid composition profile along the height of the column [24]. It is important to note that a differentiation based on the composition trajectories is only meaningful for systems with at least three components. In case of binary mixtures, the composition trajectories are simply straight lines, since the composition of both components is connected via the summation constraint [24]. While this does not mean that the composition trajectories of the EQ and RB model are generally identical for binary mixtures, they can always be aligned by adapting the HETP values. Yet, this might require the variation of HETP values along the column height (cf. Fig. 1 left), e.g., by means of data interpolation or the application of mass transfer models [3], which is rather uncommon.

In contrast to this, aligning the composition profiles is not necessarily feasible for multicomponent mixtures, as the corresponding composition trajectories might deviate from each other in multidimensional space. This can easily be illustrated for a ternary mixture, for which the composition simplex can be represented by the Gibbs triangle – a two-dimensional plane. If the composition trajectories of the EQ and RB models traverse the Gibbs triangle on different paths (cf. Fig. 1 middle), the associated composition profiles cannot be aligned by plainly adapting the HETP values (cf. Fig. 1 right). As a consequence, such deviations are an excellent indicator for the potential need to use an RB model, as the results obtained by the EQ model and respective HETP values may be misleading.

The general consideration of composition trajectories for the discrimination of the EQ and RB model is of course not a distinct novelty, since these trajectories have been used as an aid for illustrating differences in the results of EQ and RB models in respect to experimental results in a variety of publications. Ronge [25] made a comparison of experimental and simulated composition trajectories and concluded that for distillation processes in packed columns the liquid-phase mass transfer resistance can be neglected. This assumption is quite common for distillation processes [23, 26–29]. Van Dongen and Doherty [28] compared the EQ model with a differential formulation, corresponding to an RB model with equal mass transfer rates for all components. They found that the path of the calculated composition trajectories of both models differs only close to the specified product compositions. Wahnschafft et al. [29] mentioned possible differences in the attainable product composition regions determined by the distillation lines (DL) (representing the EQ model at total reflux) and the residue curves (RC), which correspond to a RB model at total reflux with equal mass transfer rates [30]. However, they also noted that DL and RC normally do not differ significantly.

Several authors addressed the component-specific mass transfer rates of the RB models in their studies. Agarwal and Taylor [31] as well as Castillo and Towler [32] used component-specific efficiencies to explore the influence of component-specific mass transfer on the path of the composition trajectories. Since the pinch points are unaffected by component-specific mass transfer rates, the minimum reflux ratio determined by EQ and RB models are generally equivalent, assuming a sufficiently high number of equilibrium trays and respective height of the column is considered [31, 32]. Nevertheless, for a finite number of stages or column height, significant differences in the calculated minimum reflux ratios may be observed [31]. Moreover, significant differences in the calculated minimum number of stages and respective height of columns were reported for the EQ and RB models at total reflux [31]. Generally, the component-specific mass transfer rates influence the path of the RB composition trajectories qualitatively, in particular their curvature [32]. Even small differences in the component-specific mass transfer rates may have a significant impact on the path of the RB composition trajectories, as the effect of the component-specific mass transfer accumulates during the integration [32]. Pelkonen et al. [23] also investigated the effect of component-specific mass transfer rates on the path of the composition trajectories. However, for the calculation of multicomponent mass transfer rates, they used the Maxwell-Stefan equations rather than component-specific efficiencies. Additionally, they analyzed the effect of different VLE models and parameter sets on the agreement of the simulated composition trajectories with experimental ones. In general, the path of the composition

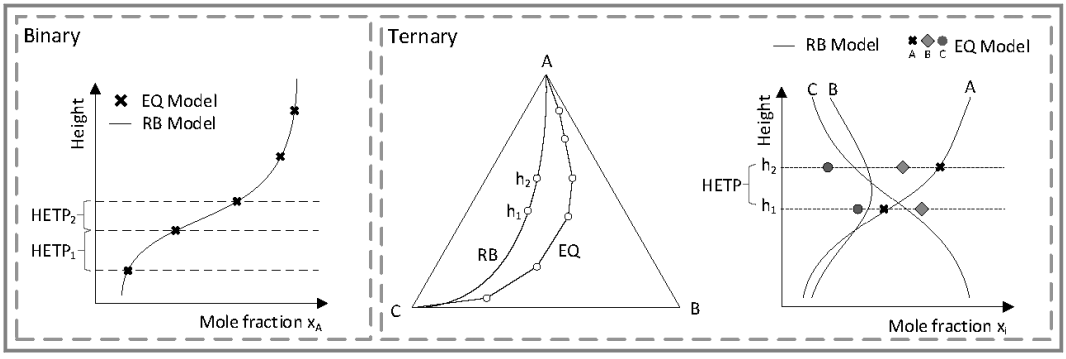

Figure 1. Depiction of the possible differences between the composition profiles of the EQ and RB models inside a distillation column for binary (left) and ternary mixtures (right).

trajectories was reported to be very sensitive to changes in the VLE model and the considered set of parameters [12, 23]. Moreover, the RB model using the Maxwell-Stefan equations showed the best match with their experimental data for the chosen VLE model and parameter set, surpassing the EQ model as well as an RB model using equal mass transfer rates for all components [23].

Moreover, Taylor et al. [27] presented a general framework for the calculation of RB composition trajectories at total reflux. Their target was to investigate the influence of component-specific mass transfer rates calculated by the Maxwell-Stefan equations on the path of the RB composition trajectories. The differences in the RB model composition trajectories with and without component-specific mass transfer rates were quantified by the relative arc length of the corresponding trajectories as well as the angle between their respective composition vectors. While the stationary points of the mixture are determined by the VLE alone, the precise path of the distillation boundaries in the composition simplex calculated by the RB model is also affected by component-specific mass transfer rates [27]. Baur et al. [26] extended this framework to finite reflux and investigated the consequences of component-specific mass transfer rates on the column design. They showed that the minimum reflux ratio is only the same for very sharp splits, while for less sharp splits with trace impurities in the products, component-specific mass transfer rates may affect the minimum reflux ratio significantly. However, Taylor et al. [27] and Baur et al. [26] did not include the EQ model in their investigations.

While the EQ and RB models can be discriminated through simulation studies, real distillation experiments are required to validate the theoretical results and to prove the superiority of one model over the other. Nevertheless, there is only a limited amount of data on experimental composition profiles of distillation in packed columns in the open literature [22, 33–35]. On the contrary, the data base of experimental profiles of tray columns is significantly larger. Particularly interesting is the work of Springer et al. [36], who investigated the differences in distillation boundaries determined based on the EQ and RB models. In a first step they evaluated the potential cutting of the total reflux boundary, which is based on the limiting DL determined by the EQ model [37], cross a composition trajectory determined by a RB model considering diffusion based on the Maxwell-Stefan equations. Subsequently, they validated their simulations by distillation experiments in a tray column for various multicomponent mixtures [38–42]. It is important to note that an evaluation of the corresponding component-specific Murphree efficiencies, based on the results of the RB model, revealed that the efficiencies vary significantly for the individual components [42] and that they are not bounded between zero and one [40]. Moreover, Springer et al. [40] could quantify the contribution of the liquid phase to the overall mass transfer resistance to less than 10 % for their experiments. Despite these interesting results it needs to be noted that all these investigations were focused on the deviation of the composition trajectories in the vicinity of distillation boundaries, which is important for the evaluation of feasible products, while no general discrimination between the EQ and RB models was pursued.

In summary, it can be concluded that most of the previous studies put a particular focus on the investigation of the component-specific mass transfer rates for the RB model. Although the results of RB models with and without component-specific mass transfer rates were compared several times, comparisons of these models with the EQ model were only conducted by Pelkonen et al. [23] for packed columns and Springer et al. [36, 38–42] for tray columns. Yet, the preceding works clearly demonstrated that the results of the EQ and RB models may differ significantly. However, it is still not clear for which mixtures and under which process parameters these differences are to be expected. In order to identify such conditions, the current publication proposes a simplified algorithmic test that allows for a systematic discrimination of the EQ and RB models.

3 Methodology

In the following section the equations for calculating the composition trajectories are derived first, before the maximum value of the shortest Euclidean distance between EQ and RB composition trajectories is presented and proposed as criterion for model discrimination.

3.1 Calculation of the Composition Trajectories

The different composition trajectories used in this work can be derived from a material balance around a differential element within a section of the packed distillation column [5, 23]

$$(V + \mathrm{d}V)(\vec{y} + \mathrm{d}\vec{y}) - V\vec{y} = V\,\mathrm{d}\vec{y} + \mathrm{d}V\,\vec{y} + \mathrm{d}V\,\mathrm{d}\vec{y} = -\vec{N}\,\mathrm{d}A \tag{1}$$

In combination with the definition of the vector of molar fluxes

$$\vec{N} = \left(\vec{J}^{V} + \vec{y}N_{\mathrm{t}}\right) \tag{2}$$

the interfacial area for mass transfer in the differential element

$$\mathrm{d}A = aA_{\mathrm{c}}\mathrm{d}z \tag{3}$$

as well as the total material balance ($\mathrm{d}V = -N_{\mathrm{t}}\mathrm{d}A$) and the negligence of the second order term ($\mathrm{d}V\mathrm{d}\vec{y}$), the integration of Eq. (1)–(3) yields

$$V\,\mathrm{d}\vec{y} = -\vec{J}^{\mathrm{V}} a A_{\mathrm{c}}\,\mathrm{d}z \tag{4}$$

where z is the axial coordinate of the packing, V is the molar vapor flow rate, $\vec{y}$ the composition vector of the bulk vapor phase. The variables A_{c} and a represent the cross-sectional area of the column and the specific interfacial area, respectively. $\vec{N}$ represents the vector of the molar fluxes, oriented from the vapor to the liquid phase, while $\vec{J}^{\mathrm{V}}$ and N_{t} are the vector of molar diffusion fluxes and the total molar flux between the phases. Based on the experimental investigations of Ronge [25] and similar to previous studies [23, 26–29], constant molar overflow is assumed, such that both liquid and vapor flow rates are assumed constant, while the temperatures of both vapor and liquid phase are assumed to be equal to the boiling temperature of the liquid mixture. These assumptions were, e.g., also considered by Taylor et al. [27]. Determining the diffusional molar fluxes based on the Maxwell-Stefan equations

$$\vec{J}^{\mathrm{V}} = c_{\mathrm{t}}^{\mathrm{V}}\left[k^{\mathrm{V}}\right]\cdot\left(\vec{y}-\vec{y}^{\mathrm{I}}\right) \tag{5}$$

with $c_{\mathrm{t}}^{\mathrm{V}}$ being the total molar vapor concentration, $[k^{\mathrm{V}}]$ being the matrix of the vapor-phase mass transfer coefficients and $\vec{y}^{\mathrm{I}}$ being the vector of vapor composition at the phase interface, yields in combination with Eq. (4)

$$V\frac{\mathrm{d}\vec{y}}{\mathrm{d}z} = c_{\mathrm{t}}^{\mathrm{V}} A_{\mathrm{c}} a\left[k^{\mathrm{V}}\right]\cdot\left(\vec{y}^{\mathrm{I}}-\vec{y}\right) \tag{6}$$

Based on the assumption of a negligible liquid-side mass transfer resistance this equation is further refined to

$$V\frac{\mathrm{d}\vec{y}}{\mathrm{d}z} = c_{\mathrm{t}}^{\mathrm{V}} A_{\mathrm{c}} a\left[k^{\mathrm{V}}\right]\cdot\left(\vec{y}^{\mathrm{EQ}}-\vec{y}\right) \tag{7}$$

as the vector of vapor compositions at the phase interface can be replaced by the vector of the equilibrium vapor compositions $\vec{y}^{\mathrm{EQ}}$ in respect to the liquid bulk composition $\vec{x}$ and thereby determined by the corresponding vapor-liquid equilibrium (VLE) conditions at the given pressure p

$$\vec{y}^{\mathrm{EQ}} = f_{\mathrm{VLE}}(\vec{x}, p) \tag{8}$$

The matrix of the vapor-phase mass transfer coefficients $[k^{\mathrm{V}}]$ can further be calculated according to [5]

$$\left[k^{\mathrm{V}}\right] = [R]^{-1}[\Gamma] \tag{9}$$

$$R_{\mathrm{ii}} = \frac{y_{\mathrm{i}}^{\mathrm{avg}}}{\kappa_{\mathrm{in}}^{\mathrm{V}}} + \sum_{\substack{\mathrm{k}=1\\ \mathrm{i}\neq\mathrm{k}}}^{\mathrm{n}} \frac{y_{\mathrm{k}}^{\mathrm{avg}}}{\kappa_{\mathrm{ik}}^{\mathrm{V}}} \tag{10}$$

$$R_{\mathrm{ij}} = -y_{\mathrm{i}}^{\mathrm{avg}}\left(\frac{1}{\kappa_{\mathrm{ij}}^{\mathrm{V}}} - \frac{1}{\kappa_{\mathrm{in}}^{\mathrm{V}}}\right) \tag{11}$$

where $\kappa_{\mathrm{ij}}^{\mathrm{V}}$ are the binary vapor-phase mass transfer coefficients, and $y_{\mathrm{i}}^{\mathrm{avg}}$ is the average vapor composition of component i according to the linearized theory [5]. Thus, $\vec{y}^{\mathrm{avg}}$ is determined as the arithmetic mean of the vapor composition in the bulk phase $\vec{y}$ and at the interface $\vec{y}^{\mathrm{I}}$, which is equivalent to the equilibrium vapor composition $\vec{y}^{\mathrm{EQ}}$ in case of the assumed negligible liquid-side mass transfer resistance. Based on the assumption of a thermodynamically ideal vapor phase, the thermodynamic correction matrix $[\Gamma]$ is furthermore assumed to be equal to the identity matrix $[I]$ in the scope of the current study. The binary vapor-phase mass transfer coefficients $\kappa_{\mathrm{ij}}^{\mathrm{V}}$ can be calculated by different mass transfer correlations [43]. Nearly all of these correlations can be rearranged into the following form [23]

$$\kappa_{\mathrm{ij}}^{\mathrm{V}} = C\left(\mathcal{D}_{\mathrm{ij}}^{\mathrm{V}}\right)^{2/3} \tag{12}$$

where C is a function of the different physical properties of the processed mixture, packing specific constants and the hydrodynamic conditions [27]. This coefficient is, however, equal for all components in the mixture. As a consequence, the binary Maxwell-Stefan vapor diffusion coefficients $\mathcal{D}_{\mathrm{ij}}^{\mathrm{V}}$ are the only component specific property required for the calculation of the relative difference between the individual mass transfer coefficients. Assuming an ideal gas phase, these $\mathcal{D}_{\mathrm{ij}}^{\mathrm{V}}$ become equal to the binary Fickian diffusion coefficients [5] and thus, are independent of the mixture composition. Following the well-known HTU-NTU approach [11] a reference height of a transfer unit, $HTU_{\mathrm{Ref}}^{\mathrm{V}}$ can be introduced

$$HTU_{\mathrm{Ref}}^{\mathrm{V}} = \frac{V}{k_{\mathrm{Ref}}^{\mathrm{V}} c_{\mathrm{t}}^{\mathrm{V}} A_{\mathrm{c}} a} \tag{13}$$

such that $\mathrm{d}z$ can be replaced by

$$\mathrm{d}z = HTU_{\mathrm{Ref}}^{\mathrm{V}}\,\mathrm{d}NTU_{\mathrm{Ref}}^{\mathrm{V}} \tag{14}$$

Assuming that the total molar vapor concentration $c_{\mathrm{t}}^{\mathrm{V}}$, cross sectional area A_{C} and the specific interfacial area a are constant along the packing height, the integration of Eqs. (7) and (14) yields

$$\frac{\mathrm{d}\vec{y}}{\mathrm{d}NTU_{\mathrm{Ref}}^{\mathrm{V}}} = \frac{[k^{\mathrm{V}}]}{k_{\mathrm{Ref}}^{\mathrm{V}}}\cdot\left(\vec{y}^{\mathrm{EQ}}-\vec{y}\right) \tag{15}$$

Thus, the dimensionless number of transfer units $NTU_{\mathrm{Ref}}^{\mathrm{V}}$ replaces the local height coordinate z as integration variable. Similar to the binary mass transfer coefficients $\kappa_{\mathrm{ij}}^{\mathrm{V}}$, the newly introduced reference mass transfer coefficient $k_{\mathrm{Ref}}^{\mathrm{V}}$ can be calculated by a correlation following Eq. (12)

$$k_{\mathrm{Ref}}^{\mathrm{V}} = C\left(D_{\mathrm{Ref}}^{\mathrm{V}}\right)^{\frac{2}{3}} \tag{16}$$

where $D_{\mathrm{Ref}}^{\mathrm{V}}$ represents a reference diffusion coefficient. Thus, due to the division of $[k^{\mathrm{V}}]$ by $k_{\mathrm{Ref}}^{\mathrm{V}}$ the computation of

the vapor composition in terms of the dimensional number of transfer units according to Eq. (15) depends solely on the binary Maxwell-Stefan vapor diffusion coefficients $Đ_{ij}^{V}$ and the VLE model used for the calculation of the vector $\vec{y}^{EQ}$ according to Eq. (8), while the actual choice of D_{Ref}^{V} only affects scales with the integration variable NTU_{Ref}^{V} and does not influence the path of the composition trajectory. The binary Maxwell-Stefan vapor diffusion coefficients $Đ_{ij}^{V}$ can be calculated by different correlations, e.g., the methods of Wilke and Lee [44] or Fuller et al. [45]. Both methods require only a few component-specific parameters, i.e., the individual boiling points and molar weights as well as the specific liquid molar volumes of the individual components (Wilke and Lee [44]) or their chemical formulas (Fuller et al. [45]).

For total reflux operation, as considered in the current article, the liquid and vapor molar flowrates are equivalent ($L = V$), such that also the vector of the liquid and vapor compositions equate at any intersection along the column height [23]

$$\vec{y} = \vec{x} \tag{17}$$

Thereby, the resulting differential equation system for the composition trajectory of the liquid phase can be derived from Eq. (15) and (17) to yield

$$\frac{\mathrm{d}\vec{x}}{\mathrm{d}NTU_{Ref}^{V}} = \frac{[k^{V}]}{k_{Ref}^{V}} \cdot \left(\vec{y}^{EQ} - \vec{x}\right) \tag{18}$$

This model is further denoted as rate-based Maxwell-Stefan (RB-MS) model, accounting for the previously introduced assumptions of constant molar overflow, a negligible liquid-side mass transfer resistance and total reflux operation. While in this study also the assumption of an ideal vapor phase is considered, necessary modification for consideration of non-ideality in the vapor phase would only affect the computation of $[k^{V}]$ through $[\Gamma]$ and $\vec{y}^{EQ}$ according to the VLE model. The derived model is essentially identical to the diffusion rectification line model considered in the work of Pelkonen et al. [23] and the total reflux model for packed columns considered by Taylor et al. [27].

In case all binary diffusion coefficients $Đ_{ij}^{V}$ are equal, the off-diagonal elements of the matrix $[k^{V}]$ vanish according to Eqs. (9)–(11) and the diagonal elements of $[k^{V}]$ become equal. Consequently, k^{V} can be factored out as a coefficient, yielding

$$\frac{\mathrm{d}\vec{x}}{\mathrm{d}NTU_{Ref}^{V}} = \frac{k^{V}}{k_{Ref}^{V}}[I] \cdot \left(\vec{y}^{EQ} - \vec{x}\right) \tag{19}$$

with $[I]$ being the identity matrix. By division of both sides of the equation with k^{V}/k_{Ref}^{V} and lumping $\mathrm{d}NTU_{Ref}^{V}k_{Ref}^{V}/k^{V}$ into a new integration variable $\mathrm{d}NTU$ the well-known Rayleigh equation for the computation of residue curve (RC) is derived

$$\frac{\mathrm{d}\vec{x}}{\mathrm{d}NTU^{V}} = \vec{y}^{EQ} - \vec{x} \tag{20}$$

This model is further denoted as rate based equal mass transfer (RB-EMT) model [27]. In accordance with this derivation, the RC model can be interpreted as a simplified rate-based model, considering CMO, for which the liquid-phase mass transfer resistance is negligible and all binary diffusion coefficients are equal [30].

The differential equations for the RB-EMT model can further be solved by means of a finite difference approximation using the Euler method [46], yielding the following equation for a step size of ΔNTU

$$\vec{x}^{(n+1)} = \vec{x}^{(n)} + \Delta NTU\left(\vec{y}^{EQ} - \vec{x}^{(n)}\right) \tag{21}$$

which results in the well-known EQ model for the computation of the DL when $\Delta NTU \rightarrow 1$

$$\vec{x}^{(n+1)} = \vec{y}^{EQ}(\vec{x}^{n}) \tag{22}$$

In this case, the superscript (n) represents a stage number for the corresponding EQ model at total reflux [47]. As illustrated in this derivation, the primary cause for the differences between the EQ model, represented by the distillation line (DL), and the RB-EMT model, represented by the RC, is the mathematical solution of the differential equation (20) by either a numerical or analytical integration or the transformation into a set of finite difference equations. As illustrated in Fig. 2a, the major differences between the resulting trajectories are, therefore, related to the fixed step size, equivalent to one equilibrium stage, for the finite difference model. Note that the DL is not equivalent to the linear connection of the finite steps, but defined as the contin-

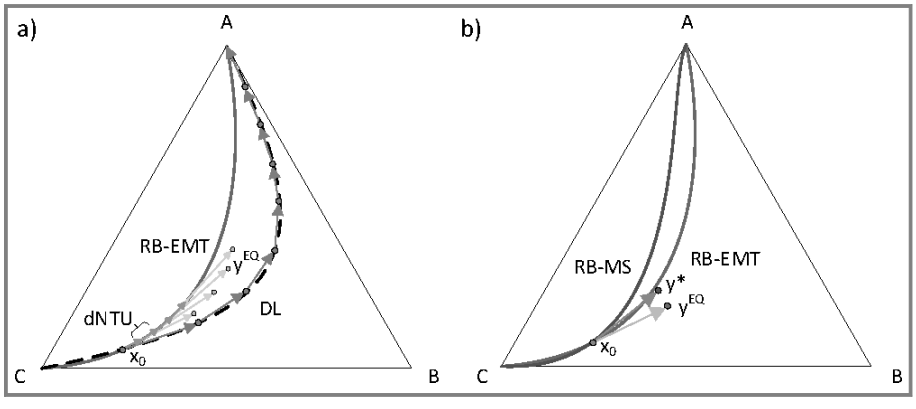

Figure 2. Depiction of the differences between the DL and RB-EMT composition trajectories due to the different calculation procedure (a) and depiction of the differences between the RB-EMT and the RB-MS composition trajectories due to component specific mass transfer rates (b).

uous trajectory of liquid compositions, for which the vapor-liquid tie lines represents chords for every composition on the trajectory [48], such that the DL is approximated by a cubic spline, as suggested by Stichlmair [49].

Since the binary diffusion coefficients are not necessarily equal for the RB-MS model, the component-specific mass transfer rates result in a deviation of the RB-MS trajectory from the RC, which is the RB-EMT trajectory. A potential increase in the deviation from the DL is illustrated exemplarily in Fig. 2b. However, it is important to note that the component-specific mass transfer rates may as well reduce the deviation from the DL, as will be discussed subsequently in Sect. 4.3.

For the presented illustrations and all further evaluations in this work, the ordinary differential equations of the RB-EMT and RB-MS models are solved numerically with MATLAB's ode45 solver, using the Dormand-Prince method. For all comparisons, the composition trajectories are calculated from the same initial composition. The integration is performed in both directions and terminated when the norm of the derivative $\frac{\mathrm{d}\vec{x}}{\mathrm{d}NTU^{\mathrm{V}}_{\mathrm{Ref}}}$ for the RB-MS model and $\frac{\mathrm{d}\vec{x}}{\mathrm{d}NTU^{\mathrm{V}}}$ for the RB-EMT model decreases below a specified threshold. The respective DLs are derived as the spline interpolation for a series of (x,p) flash calculations, starting at the same initial composition, using piecewise cubic hermite interpolation polynomials.

3.2 Quantifying the Differences Between the EQ and RB Composition Trajectories

In order to discriminate the EQ and RB models the difference between the respective composition trajectories is to be evaluated. In case of ternary mixtures, this can be performed based on a visual inspection of the different trajectories for one specific initial composition. This is illustrated in Fig. 3, for which A, B and C refer to the low, intermediate and heavy-boiling component of a general ternary mixture. It can be seen that the differences in the trajectories strongly depend on the specified initial composition. Therefore, a systematic investigation of the differences between the EQ and RB composition trajectories for a specific mixture should evaluate these differences for a large variety of initial compositions, at best covering the whole composition space. Consequently, a manual approach to such an investigation becomes infeasible.

In order to derive an algorithmic framework for the quantification of these differences between EQ and RB composition trajectories, an adequate quantitative measure that represents the largest visible difference between the composition trajectories is required. For this purpose, the maximum value of the shortest Euclidean distances d between the different trajectories is evaluated. This max-min problem is solved in two consecutive steps. First, the shortest Euclidean distance is determined by a numerical search algorithm that evaluates for each composition on one trajectory the closest composition on the respective other trajectory. Second, the maximum value d of all the calculated shortest Euclidian distances is evaluated. While this is a robust approach that works well for the considered systems and a large number of initial compositions, a direct simultaneous solution of the respective max-min problem may be more effective for large multicomponent systems.

For ternary mixtures, the results of the solution of the max-min problem for a multitude of initial compositions can be plotted in a ternary contour plot. The derivation of the maximum value d of the minimum Euclidian distance and the resulting contour plot for a full coverage of the composition space is illustrated in Fig. 4, considering an ideal mixture with constant relative volatilities. The dark blue areas in the contour plot (Fig. 4d) represent the initial compositions for which the differences between the EQ and MS trajectories are comparably small. The areas with colors from green to red represent initial compositions for which the maximum Euclidian distance d between the EQ and RB composition trajectories are increasing. For illustration purpose, Fig. 4c depicts the DL and RB-EMT trajectories, as well as the respective maximum of the shortest Euclidian distance between them, for one initial composition that results in a fairly large difference between the trajectories. The contour plot allows for a direct evaluation of the differences between the EQ and RB composition trajectories for the whole mixture. Moreover, regions in the composition simplex for which the differences between the EQ and RB-EMT or RB-MS trajectories are the most significant can be identified easily.

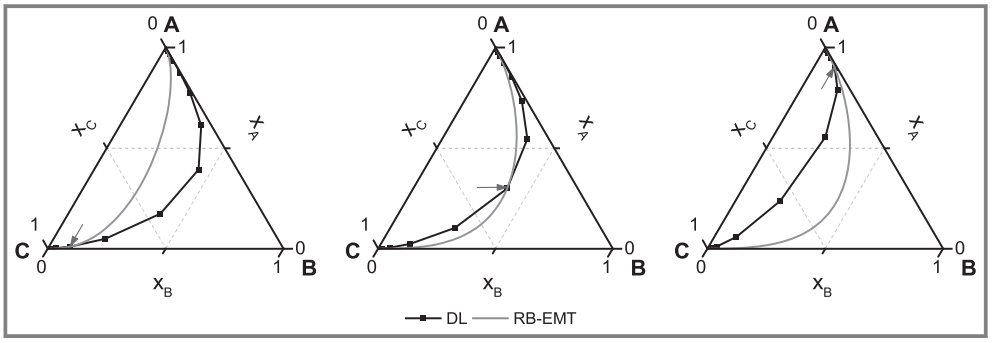

Figure 3. Exemplary paths of the DL and RB-EMT compositions trajectories for three different initial compositions of the trajectories. The arrows indicate the initial compositions.

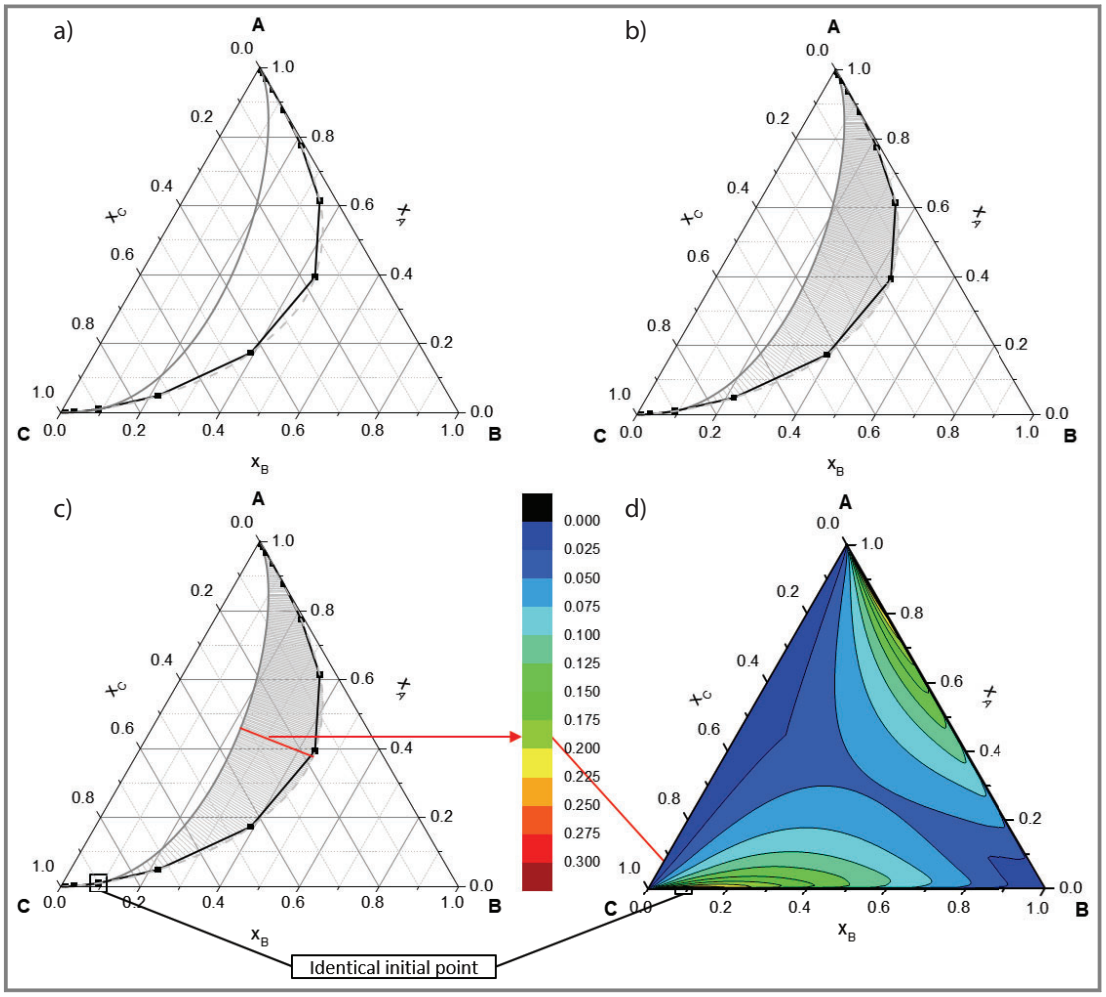

Figure 4. Calculation procedure for the maximum value of the shortest Euclidean distances, *d*, between the EQ and RB composition trajectories and subsequent illustration by means of a ternary contour plot.

In order to guarantee a high resolution of the composition space, 12 150 initial compositions were evaluated for each of the depicted contour plots in the current paper. Due to the larger variations close the binary edges, the distribution is non-uniform with a higher resolution close to the binary edges and a lower resolution close to the center of the composition space. Note that the algorithmic approach for the computation of the maximum value of the shortest Euclidean distance *d* is not limited to ternary mixtures but can be applied to mixtures with an arbitrary number of components. Yet, for the sake of visualization of the results, the current article focusses on the application to ternary mixtures.

4 Theoretical Model Discrimination

Building on the presented algorithmic approach for the quantification of the differences between the EQ and RB trajectories, the subsequent investigation first evaluates the effect of the relative volatilities for ideal mixtures, as well as component-specific mass transfer rates, before evaluating the transferability of derived criteria for considerable differences between EQ and RB trajectories for two real mixtures. First, the contour plots are used to discriminate the EQ and RB models for ideal mixtures.

4.1 Influence of the VLE on the Deviation of the EQ and RB-EMT Composition Trajectories

The EQ and RB-EMT models, which result in the DL and RC, require only information about the VLE, as it is assumed that all binary diffusion coefficients $Đ_{ij}^{V}$ are equal (cf. Sect. 3.1). In this first stage of the investigations the VLE is calculated based on constant relative volatilities (CRV). This enables a simple and targeted modification of the VLE. The CRV of the binary submixtures are always denoted in the following form:

$$\vec{\alpha} = (\alpha_{AB} \quad \alpha_{AC} \quad \alpha_{BC}) \tag{23}$$

Only two of the binary CRV can be specified independently, since the third one is computed as the ratio of the other two. Here, α_{AC} and α_{BC} are specified while α_{AB} is calculated as the ratio of the former two. In the following, the influence of the VLE on the differences between the EQ and RB-EMT composition trajectories is analyzed by evaluation of contour plots for different sets of relative volatilities.

Fig. 5 illustrates respective contour plots determined for mixtures, for which the relative volatility α_{AC} is fixed at 6, while α_{BC} is varied from 2 to 4. As such, the first two mixtures are characterized as wide-boiling, since all relative volatilities larger or equal to 2, while the third mixture is partially close-boiling (α_{AB}) and wide-boiling ($\alpha_{AC} > \alpha_{BC} > 2$). The smallest deviation between the EQ and RB-EMT trajectories are determined for initial compositions with very high or very low amounts of the intermediate boiling component B. Furthermore, almost equimolar initial compositions result in comparably small deviations. The largest deviations are determined for low compositions of low boiler A or high boiler C, close to the binary edges. However, the shape of the regions of higher deviations deforms with the variation of α_{BC}. While the shape of both regions is rather symmetrical for $\alpha_{BC} = 3$ (cf. Fig. 5b), the lower regions flattens towards the binary BC edge and the upper region deforms towards the low boiler A in case of a reduced relative volatility (cf. Fig. 5a), while the upper region flattens towards the binary AC edge and the lower region deforms towards the high boiler C in case of an increased volatility (cf. Fig. 5c).

However, it is important to note that the regions of higher deviations do not extend towards the binary edges, as there are no differences in the EQ and RB trajectories for the binary subsystems ($d = 0$). Consequently, the contour lines are closed close to the binary edges, although this is hardly visible in the contour plot.

While the maximum deviations between the EQ and RB-EMT model reached values in the Eucledian distance of 0.15 for noticeable regions of the composition space, in case of the relatively wide boiling mixtures, these deviations are

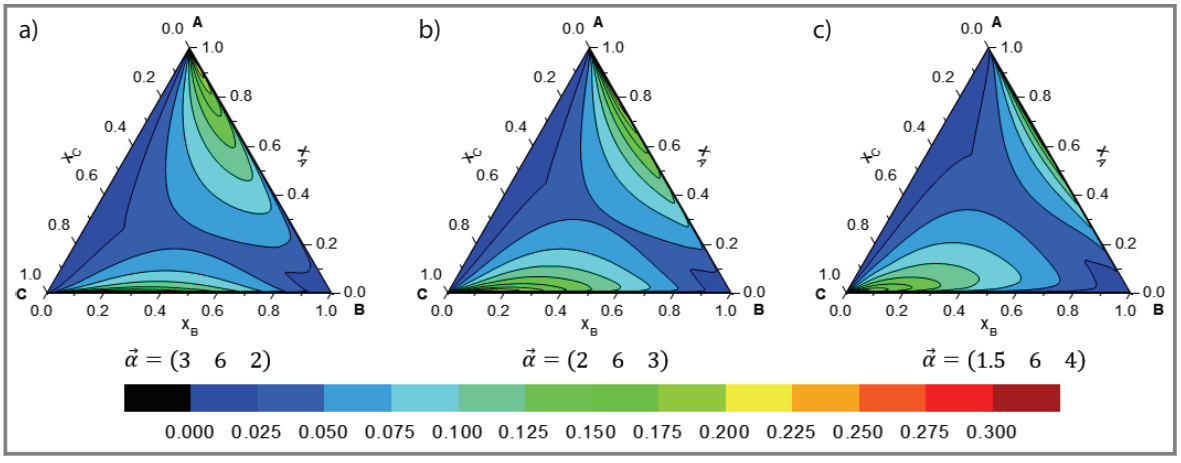

Figure 5. Contour plots illustrating the distance *d* values between the DL and RB-EMT composition trajectories for three mixtures, α_{AC} is fixed at 6 while α_{BC} is varied.

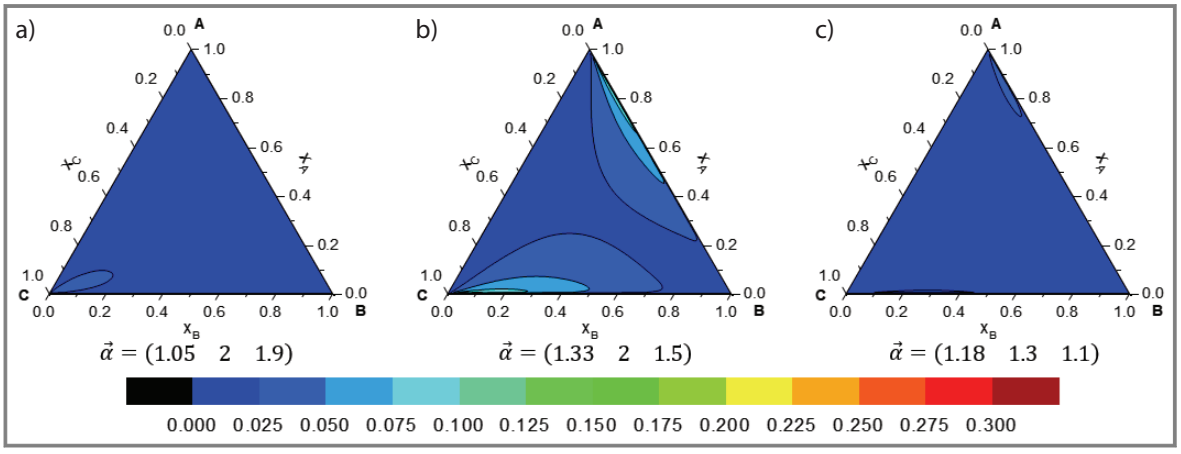

Figure 6. Contour plots for several combinations of the relative volatilities with $\alpha_{ij} \leq 2$ illustrating the distance *d* values between the DL and RB-EMT composition trajectories.

reduced significantly for closer boiling mixtures, as illustrated in Fig. 6 for which all relative volatilities are below or equal to 2. Especially for the very narrow-boiling mixture with the contour plot illustrated in Fig. 6c almost no recognizable deviation becomes apparent.

Consequently, it can be concluded that the differences between the EQ and RB-EMT composition trajectories are very small for close-boiling mixtures and increase in specific regions of the composition space for wider-boiling mixtures. This observation from the contour plots aligns perfectly with statements in related publications, as e.g., Taylor [7] pointed out that the EQ model can fail to adequately describe especially high-relative-volatility distillation and some very high purity separations. The large difference between the EQ and RB-EMT composition trajectories for wide-boiling mixtures results directly from the large step size in the finite difference scheme of the EQ model, which is determined by the VLE. The largest differences in the DL and RB-EMT composition trajectories are located close to the edges of A and C at the binary A/B and B/C lines, while the magnitude of d depends on the relative volatility of the corresponding binary submixtures.

In order to support these conclusions, Fig. 7 depicts further contour plots for additional combinations of relative volatilities, combining low and high relative volatilities of the involved submixtures. Similar to the wide-boiling mixtures evaluated in Fig. 5, larger differences between the EQ and RB-EMT model are demonstrated by the maximum of the shortest Euclidian distance for the mixture for which all relative volatilities are larger or equal to 2 (cf. Fig. 7b). However, as illustrated by Fig. 7a and 7c, these differences are significantly smaller, indicating that the differences between the EQ and RB-EMT model for a ternary mixture are much less pronounced as long as one of the involved binary submixtures is narrow-boiling. Comparing Fig. 7a and 7c, it also becomes apparent that the significant increase of the relative volatility between the low/intermediate and the high-boiling component do merely affect the magnitude of these deviations.

In support of this conclusion, the differences between the EQ and RB-EMT composition trajectories are particularly large for mixtures, for which all binary submixtures are wide-boiling ($\alpha_{ij} \geq 2$), while the differences are much less pronounced as long as one binary submixture is close boiling. For overall close-boiling systems the differences between the DL and RB-EMT composition trajectories become negligible. While these rules are formulated based on the investigation of ideal mixtures with constant relative volatilities, they should hold also for real, zeotropic mixtures [50]. Since the EQ and RB-EMT model are reflecting the RC and DL, it can further be concluded that the oftentimes considered equivalency of DL and RC for the analysis of split feasibility [29, 46] is not adequate for the analysis of wide-boiling mixtures.

4.2 Influence of the Component-Specific Mass Transfer on the Deviation of the EQ and RB-EMT Composition Trajectories

After evaluating the effect of the VLE on the differences between the EQ and RB-EMT composition trajectories, the effect of component-specific mass transfer rates is evaluated by an investigation of the RB-MS model, in respect to the other two models. For this investigation the VLE is still modeled based on CRV. For the subsequent analysis the three binary Maxwell-Stefan vapor-phase diffusion coefficients $Đ_{ij}^{V}$ for the ternary mixtures are varied systematically to evaluate their influence on the differences in the EQ and RB composition trajectories. It is important to note that the course of the RB-MS composition trajectories is not affected by the absolute values of $Đ_{ij}^{V}$, but only by the ratios between the individual $Đ_{ij}^{V}$. Thus, for the reference case (RB-EMT) all $Đ_{ij}^{V}$ are set to unity and further varied individually

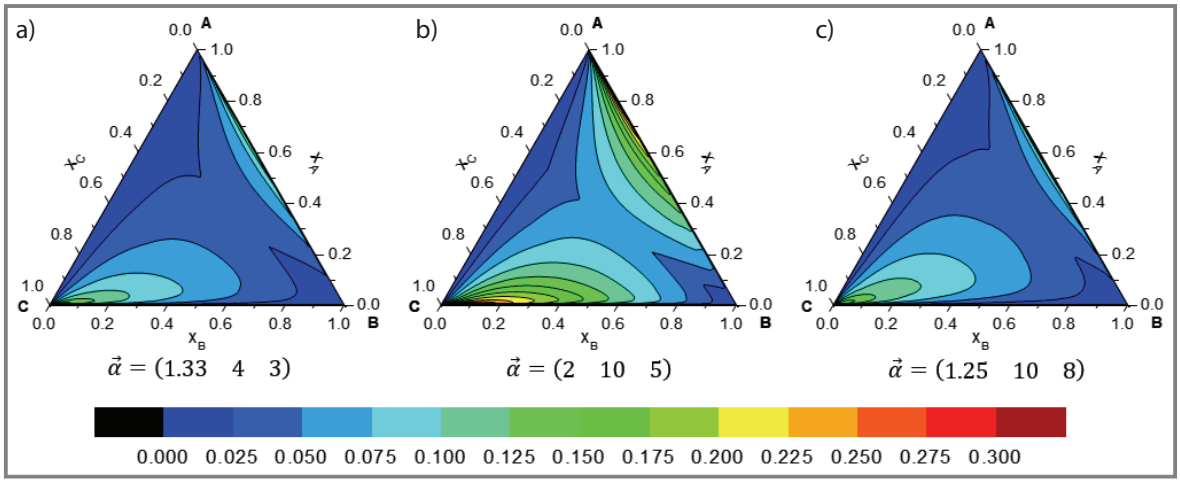

Figure 7. Contour plots of further ideal mixtures illustrating the distance d values between the DL and RB-EMT composition trajectories.

by ± 50 % (RB-MS). Since only the ratios of the diffusion coefficients are relevant, a variation of two of the three diffusion coefficients is sufficient. The relative volatilities are fixed to $\vec{\alpha} = (2 \quad 6 \quad 3)$ while the set of binary Maxwell-Stefan vapor diffusion coefficients $Đ_{ij}^{V}$ is reported as:

$$\vec{Đ} = (Đ_{AB} \quad Đ_{AC} \quad Đ_{BC}) \tag{24}$$

The resulting contour plots for all considered combinations of modified diffusion coefficients are illustrated in Fig. 8. While the diffusion coefficient $Đ_{AB}$ is kept constant, the top three contour plots represent the effect of an increased $Đ_{AC}$ (Figs. 8a–c), while the bottom three contour plots illustrate the effect of a decreased $Đ_{AC}$ (Figs. 8g–i). Similarly, the three contour plots on the left side illustrate the effect of a decreased $Đ_{BC}$ (Figs. 8a,d,g), while the three contour plots on the right side illustrate the effect of an increased $Đ_{BC}$ (Figs. 8c,f,i).

Apparently, the deviation of the EQ and RB-MS composition trajectories becomes more pronounced for decreased $Đ_{AC}$ and $Đ_{BC}$ values, while it gets less pronounced in case of increased $Đ_{AC}$ and $Đ_{BC}$ values. Judging from the difference in Fig. 8a and 8i the value of $Đ_{BC}$ has a more pronounced effect on the RB-MS composition trajectories than the $Đ_{AC}$ value. However, the general structure of the contour plots remains the same, since the topology of the VLE is not affected by the variation of the individual mass transfer rates [26].

As described in Sect. 3.1 the sole difference between the EQ and RB-EMT model results from the different approach for solving the differential equation (20) by either a numerical or analytical integration or the transformation into a set of finite difference equations. Geometrically the deviation between the resulting DL and RC can be explained by the evaluation of the vapor-liquid tie-line (straight line connecting $\vec{x}$ and $\vec{y}^{EQ}(\vec{x})$), which represents the tangent to the RC but a secant

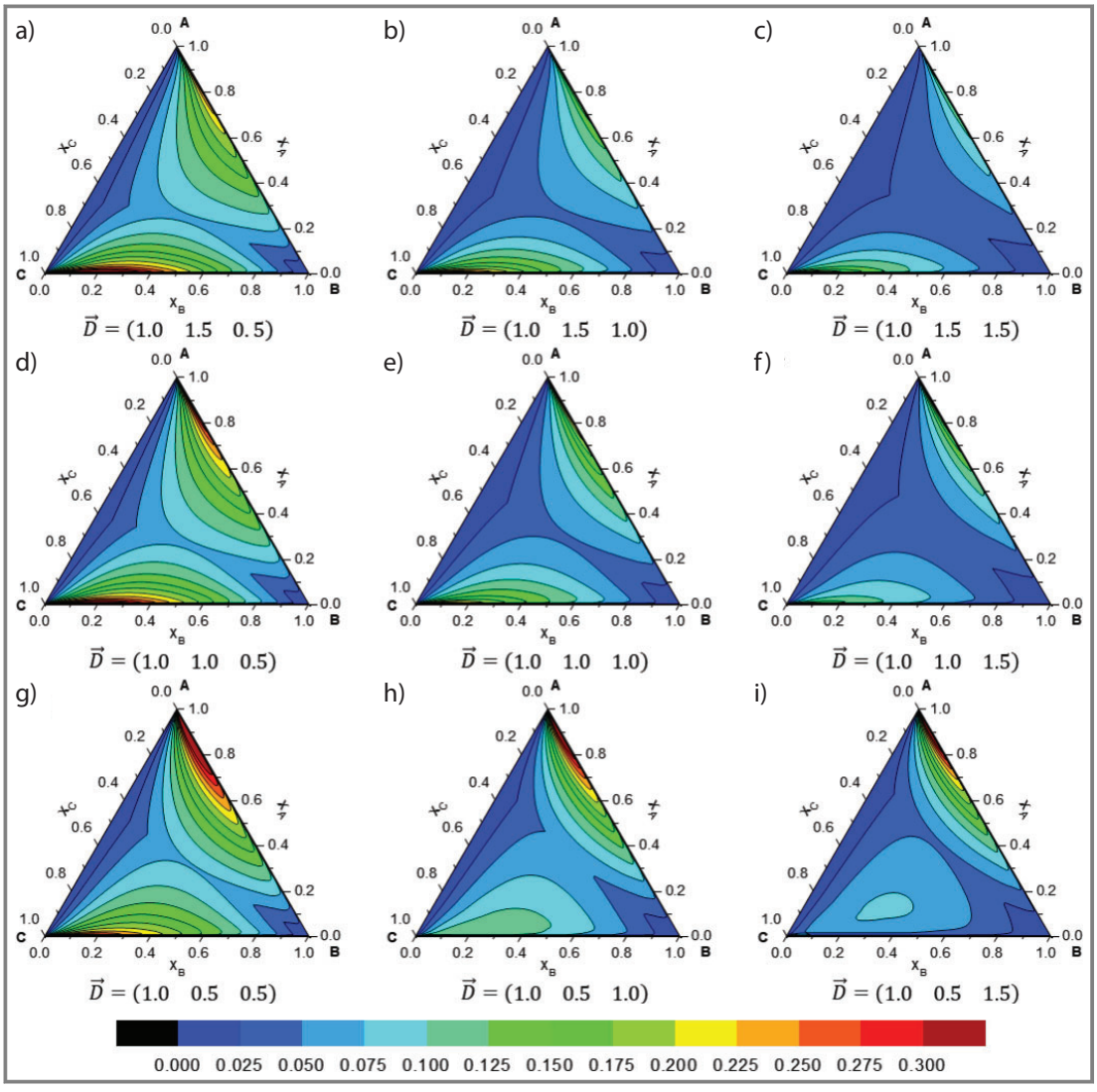

Figure 8. Several contour plots illustrating the distance *d* values between the DL and RB-MS composition trajectories for varying binary vapor-phase diffusion coefficients for an ideal mixture with relative volatilities α = (2 6 3).

to the DL passing through $\vec{x}$ [48]. In case of the RB-MS model, the tangent to the resulting composition trajectory is altered in magnitude and direction by multiplication with the matrix of the vapor-phase mass transfer coefficients [k^V]. This modification can either increase the deviation from the EQ model, as illustrated in Fig. 2b, or reduce the deviation in case the integration of the differential equation (18) results in a trajectory that traverses closer to the DL. While general conclusions on the effect of a specific relation of the binary Maxwell-Stefan vapor diffusion coefficients may not be derived from the current results, the proposed evaluation of the maximum value of the shortest Euclidean distances and the illustration in terms of the contour plots for ternary mixtures presents an efficient tool enabling a case-specific evaluation.

4.3 Evaluation of the Transferability to Real Mixtures

In order to illustrate the applicability of the approach and showcase the transferability of the results, the respective contour plots are computed for two real mixtures, which are expected to show large differences in the EQ and RB composition trajectories according to the derived criteria. For both considered mixtures the VLE calculations are performed for a constant atmospheric pressure using the UNIQUAC g^E model and the extended Antoine equation. Furthermore, the correlation of Wilke and Lee [44] is used to calculate the binary vapor diffusion coefficients.

4.3.1 Methanol – 2-Butanol – DMF

At first a ternary mixture of methanol (MeOH), 2-butanol (2-BuOH) and dimethylformamide (DMF), abbreviated as MBD, is investigated. The required property parameters are extracted from the Aspen Plus® databases NISTV88 NIST-IG and PURE32. The resulting relative volatilities and the normalized binary vapor diffusion coefficients are listed in Tab. 1 for three liquid compositions in the vicinity of the pure components, while the averaged values present the arithmetic mean for all 12 150 liquid compositions evaluated for the generation of the contour plots illustrated in Fig. 9.

Table 1. Averaged relative volatilities and normalized diffusivities for the MBD mixture.

Parameter	Values			Averaged
Mole fraction				
x_{MeOH} [–]	0.990	0.005	0.005	
$x_{2\text{-BuOH}}$ [–]	0.005	0.990	0.005	
x_{DMF} [–]	0.005	0.005	0.990	
Relative volatility				
$\alpha_{MeOH,DMF}$ [–]	41.71	16.81	9.29	18.92
$\alpha_{2\text{-BuOH,DMF}}$ [–]	9.07	5.23	4.38	5.97
$\alpha_{MeOH,2\text{-BuOH}}$ [–]	4.60	3.22	2.12	3.11
Normalized diffusivity				
$Đ_{MeOH,DMF}/Đ_{MeOH,2\text{-BuOH}}$ [–]	1.02	1.02	1.02	1.02
$Đ_{2\text{-BuOH,DMF}}/Đ_{MeOH,2\text{-BuOH}}$ [–]	0.59	0.59	0.59	0.59

Based on the high relative volatilities, exceeding those of the CRV mixtures investigated in Sect. 4.1, large deviations of the EQ and RB-EMT composition trajectories are expected. In case the ratio of the binary Maxwell-Stefan vapor diffusion coefficients has the same effect observed for the CRV mixture in Sect. 4.2, an even more pronounced deviation of the EQ and RB-MS composition trajectories is expected. As illustrated in Fig. 9 these expectations are met very well by the resulting contour plots. The regions that represent considerable deviations of the EQ and RB models, presented by maximum values of the shortest Euclidean distances ($d \geq 0.1$), do extend towards the center of the com-

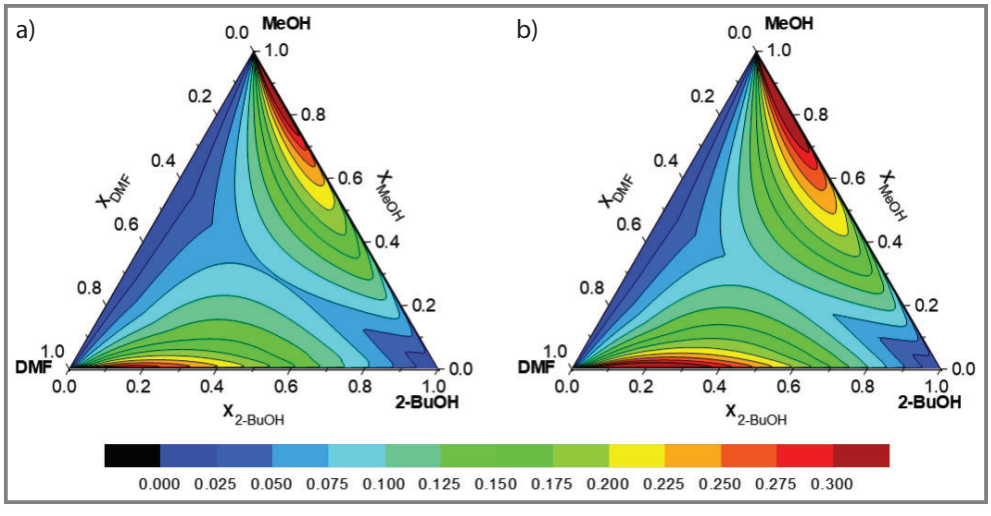

Figure 9. Contour plots for the MBD mixture illustrating the distance *d* values between a) the DL and RB-EMT composition trajectories and b) the DL and RB-MS composition trajectories.

position simplex for both the RB-EMT and RB-MS model, while especially for the latter, deviations with $d \geq 0.25$ are recognizable for large regions close to the MeOH and DMF edges on the binary MeOH-2-BuOH and 2-BuOH-DMF line. As expected, these values of the maximum of the shortest Euclidian distance are even larger than for any of the previously considered ideal mixtures in Sect. 4.1 and 4.2.

4.3.2 Acetone – Methanol – Water

The second ternary mixture to be evaluated is an azeotropic mixture of acetone, MeOH and water, abbreviated as AMW. The required property parameters are again extracted from the Aspen Plus® databases APV88 VLE-IG and PURE32. The mixture exhibits a binary, temperature-minimum azeotrope between acetone and methanol, which is illustrated in the residue curve map in Fig. 10.

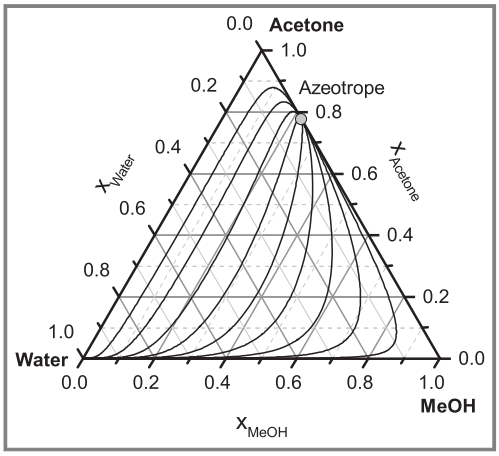

Figure 10. Residue curve map of the AMW mixture.

While the mixture does not exhibit a distillation boundary, the composition space is divided in two compartments to both sides of the azeotrope, which are characterized by a different order of the relative volatilities. This becomes apparent from the relative volatilities determined for the liquid compositions close to the pure acetone and methanol vertex, as listed in Tab. 2. Due to this shift in the order of the relative volatilities, the analysis of an average of the relative volatilities does not seem reasonable and is skipped. Yet, the indicated relative volatilities for the three liquid compositions indicate a very narrow boiling region close to the acetone vertex, as well as a quite wide boiling region close to the water edge.

While no direct conclusion can be drawn from an equivalency to a CRV mixture, the differences between the EQ and RB composition trajectories can effectively be evaluated by the computation of the maximum of the shortest Euclidian distance, for which the results are illustrated by means of the contour plots in Fig. 11. While the contour plots deviate to some extend from those of the previously investigated CRV mixtures, the low deviations of the EQ and RB-EMT model (cf. Fig. 11a) close to the acetone-MeOH edge and the higher deviations close to the water-MeOH align with the relative volatility values listed in Tab. 2. Furthermore, the reduced deviation between the EQ and RB-MS model (cf. Fig. 11b) are also to be expected when considering the normalized diffusivity values listed in Tab. 2, considering the results for the CRV mixture in Sect. 4.2.

Table 2. Averaged relative volatilities and normalized diffusivities for the AMW mixture.

Parameter	Values			Averaged
Mole fraction				
x_A [–]	0.990	0.005	0.005	
x_{MeOH} [–]	0.005	0.990	0.005	
x_W [–]	0.005	0.005	0.990	
Relative volatility				–
$\alpha_{Acetone,Water}$ [–]	1.33	5.99	21.74	–
$\alpha_{MeOH,Water}$ [–]	1.73	2.45	7.50	–
$\alpha_{Acetone,MeOH}$ [–]	0.77	2.44	2.90	–
Normalized diffusivity				
$Đ_{Acetone,Water}/Đ_{Acetone,MeOH}$ [–]	1.47	1.47	1.47	1.47
$Đ_{MeOH,Water}/Đ_{Acetone,MeOH}$ [–]	2.00	2.00	2.00	2.00

While the contour plots for the azeotropic system cannot be predicted directly from the simplified criteria derived from the analysis of the CRV mixtures, the deviations between the EQ and RB models in different regions of the composition space align well with the respective expectations. In any way, the algorithmic assessment allows for a quick evaluation of potential deviations by means of the maximum of the shortest Euclidian distance and the illustration in terms of the contour plots.

5 Experimental Validation

In order to validate the applicability of the derived criteria for the evaluation of a chemical system for which the use of an RB model is likely required due to considerable deviations from the EQ model, an experimental validation is conducted. For this purpose, real composition profiles for the distillation of the previously evaluated ternary MBD mixture were determined experimentally for total reflux experiments conducted in a special lab-scale column at BASF SE (see Fig. 12). The column had an inner diameter of 0.05 m and was equipped with Montz A3-500 gauze wire packing divided into short segments of 0.24 m height allowing a high number of dedicated sample positions. In the upper part short sampling distances were gained by the use

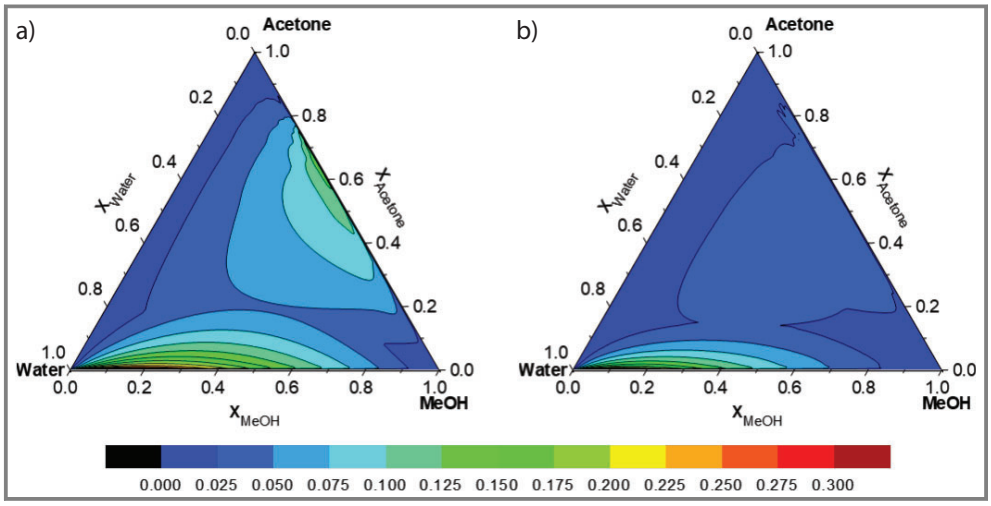

Figure 11. Contour plots for the AMW mixture illustrating the distance *d* values between a) the DL and RB-EMT composition trajectories and b) the DL and RB-MS composition trajectories.

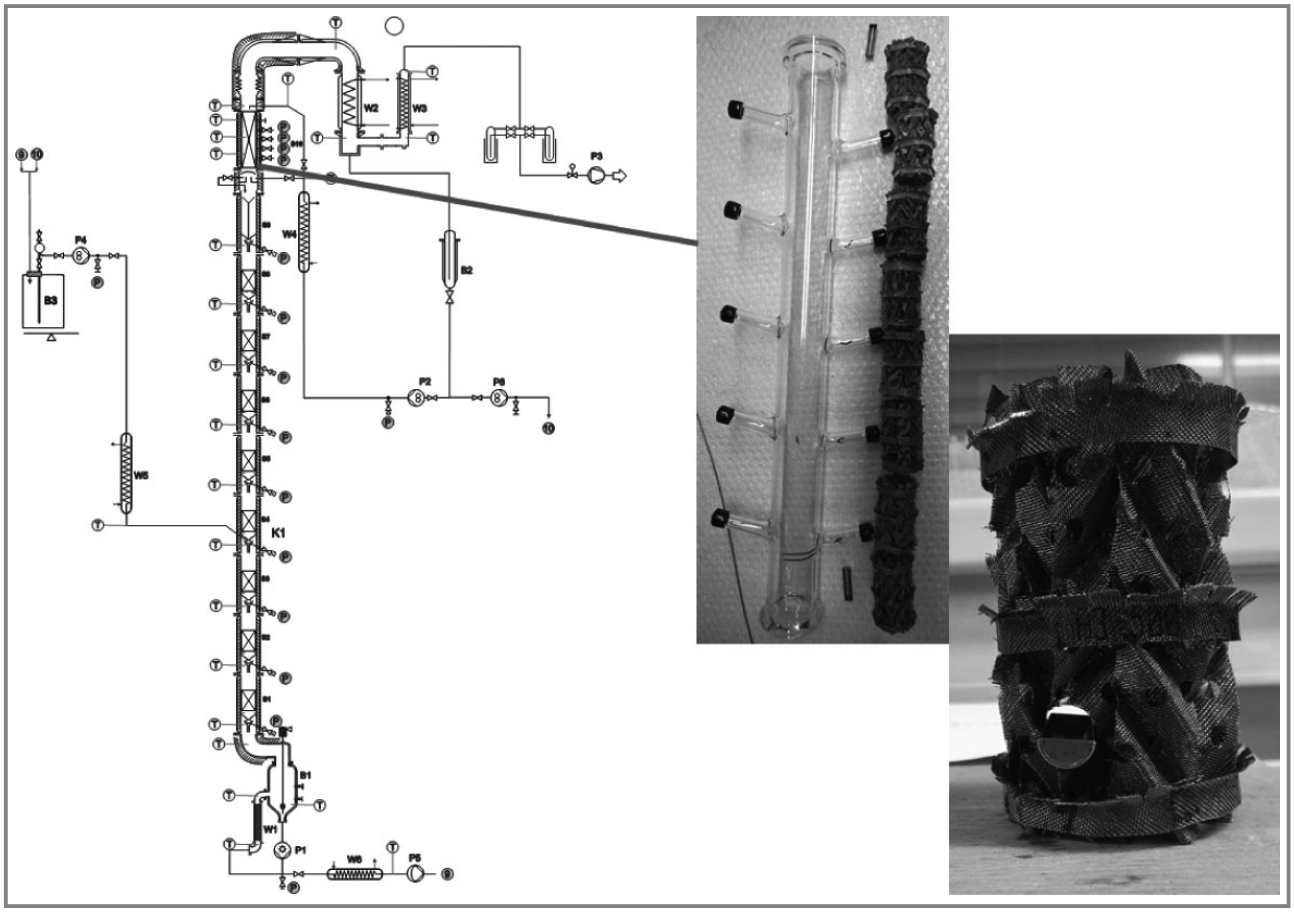

Figure 12. Experimental setup and with profile sampling locations (left side). Upper column section with special sampling pipes (middle and right).

of specially designed sampling pipes (see Fig. 12 middle and right). The performance of the column was first validated by means of a standard binary test mixture. Fig. 13 shows a comparison of experimentally determined liquid compositions along the column height with the composition trajectories resulting from the different models and three different initial compositions.

For all three of the considered initial compositions for the computation of the composition trajectories, the DL (resulting from the EQ model) provides a poor approximation of

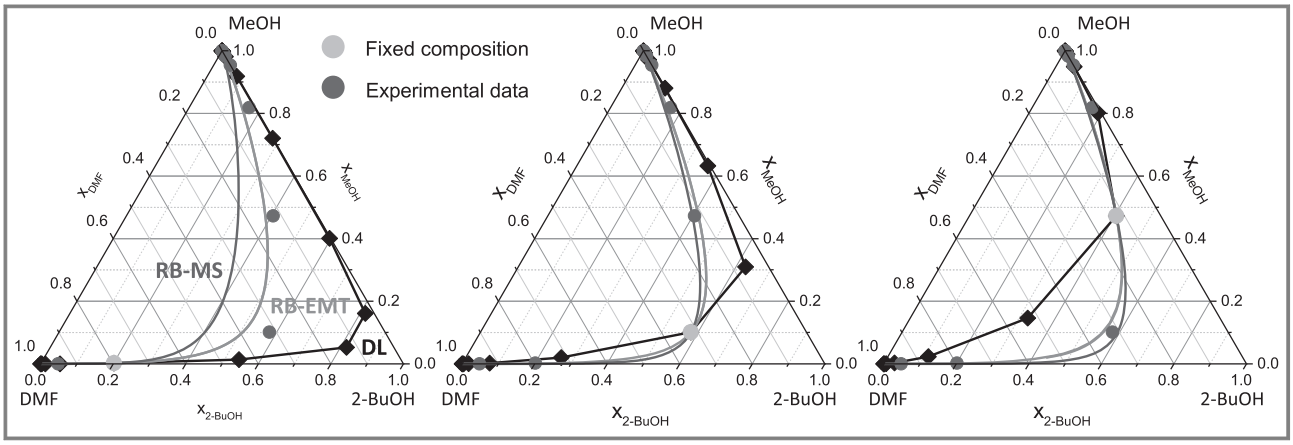

Figure 13. Comparison of the experimental data points with the calculated DL, RB-EMT, and RB-MS composition trajectories.

the experimental data. Both RB composition trajectories agree significantly better with the experimental data points. While the RB-MS trajectories match the experimental data points excellently in the middle and right diagram, the agreement with the experimental data points is, however, worse for the initial composition considered in the left diagram, when compared to the RB-EMT model. While this is rather unexpected, considering that the RB-MS model is fundamentally more sound, the deviation is likely the result of an inaccuracy of the estimated binary diffusion coefficients as well as the specific-composition measurement, for which the trajectories are specifically sensitive in this region of the composition space (cf. Fig. 9). Overall, the experimental results align well with the expectations that were derived from the model-based analysis of the MBD mixture as well as the derived criteria from the analysis of ideal mixtures. Moreover, the algorithmic methods for the derivation of the maximum values of the shortest Euclidean distances and the contour plots provide a simple means for the identification of chemical systems for which large deviations between the EQ and RB models are to be expected.

6 Conclusion and Outlook

In order to evaluate chemical systems for which the use of a rate-based model should be considered for sizing of packed distillation columns, the equilibrium stage and rate-based models for total reflux operation have been evaluated in a systematic study, considering the maximum of the shortest Euclidian distances d between the resulting liquid composition trajectories as suitable means for model discrimination. For ternary mixtures, contour plots have been developed to enable an easy graphical assessment of the resulting differences in the computed composition trajectories. Based on the considered assumptions of total reflux operation, a negligible liquid-side mass transfer resistance, constant molar overflow and an ideal vapor phase, the evaluation of the different models requires only information on the vapor-liquid equilibrium as well as the binary Maxwell-Stefan vapor diffusion coefficients, such that the developed approach can be utilized with little required information.

The conducted parameter study validated known expectations [7] that especially wide-boiling mixtures are prone to larger deviations between the equilibrium stage and rate-based models, while the expected deviations are rather small for generally close boiling mixtures. Yet, the study also showed that the expected deviations are also rather small in case at least one binary submixture of a ternary mixture is close-boiling, while the other submixtures may show large relative volatilities. Non-uniform component-specific mass transfer rates, originating from differences in the binary Maxwell-Stefan diffusion coefficients, can either increase or decrease these deviations. Although the initial observations were derived for hypothetical mixtures with constant relative volatilities, the investigations for two real mixtures validated the applicability of the derived criteria for model discrimination, even in case of azeotropic mixtures when considering individual regions of the composition space. Based on the observed significant differences between the EQ and RB composition trajectories for the MBD mixture, dedicated experiments were conducted in a lab-scale column, showcasing the superiority of the RB model over the EQ model under the specific conditions.

While the current work investigated the influence of the mixture properties on the differences between EQ and RB composition trajectories at total reflux, future work will evaluate the additional effect of finite reflux operation, for which different process parameters have to be considered in the evaluation of the differences between the EQ and RB model. Finally, the objective is an early-stage quantitative evaluation of the influence of the chosen modeling approach on the obtained column design.

This work was funded by the Deutsche Forschungsgemeinschaft (DFG, German Research Foundation) – TRR 63 "Integrated Chemical Processes in Liquid Multiphase Systems" (subproject T2 "Hybrid separation processes: Modeling and design of membrane-assisted distillation processes") – 56091768.
Gefördert durch die Deutsche Forschungsgemeinschaft (DFG) – TRR 63 „Integrierte chemische Prozesse in flüssigen Mehrphasensystemen" (Teilprojekt T2 „Hybride Trennprozesse: Modellierung und Entwurf von membrangestützter Rektifikation") – 56091768.

Symbols used

a	$[m^2m^{-3}]$	specific interfacial area
A_c	$[m^2]$	cross-sectional area of the column
c_t^V	$[mol\ m^{-3}]$	molar concentration
C	[–]	constant
d	[–]	maximum value of the shortest Euclidean distances
D	$[m^2s^{-1}]$	diffusion coefficient
$Đ$	$[m^2s^{-1}]$	Maxwell-Stefan diffusion coefficient
dz	[m]	differential height
HTU	[m]	height of a transfer unit
$[I]$	[–]	identity matrix
J	$[mol\ m^{-2}s^{-1}]$	molar diffusion flux
k	$[m\ s^{-1}]$	mass transfer coefficient
N_t	$[mol\ m^{-2}s^{-1}]$	total molar flux
NTU	[–]	number of transfer units
$[R]$	$[s\ s^{-1}]$	inverse matrix of mass transfer coefficients
V	$[mol\ s^{-1}]$	molar vapor flow rate
x	[–]	liquid molar composition
y	[–]	vapor molar composition
z	[m]	axial coordinate

Greek letters

α	[–]	relative volatility
κ	$[m\ s^{-1}]$	binary mass transfer coefficient

Sub- and Superscripts

avg	average of the bulk and interphase value
EQ	equilibrium
i, j, k, n	component number
n	stage index
OV	overall vapor
V	vapor phase

Abbreviations

2-BuOH	2-butanol
AMW	acetone, methanol, water
CMO	constant molar overflow
CRV	constant relative volatility
DMF	dimethylformamide
EMT	equal mass transfer
EQ	equilibrium stage
HETP	height equivalent to a theoretical plate
MBD	acetone, 2-butanol, dimethylformamide
MeOH	methanol
MS	Maxwell-Stefan
Ref	reference
RB	rate-based
VLE	vapor-liquid equilibrium

References

[1] E. Y. Kenig, S. Blagov, in *Distillation: fundamentals and principles* (Eds: A. Górak, E. Sorensen), Elsevier, Amsterdam **2014**.
[2] H. Z. Kister, *Distillation operation*, McGraw Hill, New York **1990**.
[3] H. Z. Kister, *Distillation design*, McGraw Hill, New York **1992**.
[4] Ż. Olujić, in *Distillation: Equipment and Processes* (Eds: A. Górak, Ż. Olujić), Academic Press, Boston **2014**.
[5] R. Taylor, R. Krishna, *Multicomponent mass transfer*, Wiley Series in Chemical Engineering, Wiley, New York **1993**.
[6] N. Kockmann, *ChemBioEng Rev.* **2014**, *1 (1)*, 40–49. DOI: https://doi.org/10.1002/cben.201300003
[7] R. Taylor, *Ind. Eng. Chem. Res.* **2007**, *46 (13)*, 4349–4357. DOI: https://doi.org/10.1021/ie061626m
[8] E. Sorel, *La Rectification de L'alcool*, Gauthier-Villars et fils, Paris **1893**.
[9] R. Taylor, R. Krishna, H. Kooijman, *Chem. Eng. Prog.* **2003**, *99 (7)*, 28–39.
[10] H. Schoenmakers, L. Spiegel, in *Distillation: Equipment and Processes* (Eds: A. Górak, Ż. Olujić), Academic Press, Boston **2014**.
[11] T. H. Chilton, A. P. Colburn, *Ind. Eng. Chem.* **1935**, *27 (3)*, 255–260. DOI: https://doi.org/10.1021/ie50303a004
[12] A. Gorak, A. Kraslawski, A. Vogelpohl, *Int. Chem. Eng.* **1990**, *30 (1)*, 1–15.
[13] A. Górak, in *Prozeßsimulation* (Ed: H. Schuler), VCH Verlag, Weinheim **1994**.
[14] E. Y. Kenig, *Chem. Eng. Res. Des.* **2008**, *86 (9)*, 1059–1072. DOI: https://doi.org/10.1016/j.cherd.2008.04.011
[15] E. Y. Kenig, *Comput. Chem. Eng.* **1997**, *21 (Suppl. 1)*, S355–S360.
[16] A. Shilkin, E. Y. Kenig, *Chem. Eng. J.* **2005**, *110 (1)*, 87–100. DOI: https://doi.org/10.1016/j.cej.2005.03.018
[17] E. Y. Kenig, *Chem. Ing. Tech.* **2011**, *83 (4)*, 443–455. DOI: https://doi.org/10.1002/cite.201000147
[18] R. Krishnamurthy, R. Taylor, *AIChE J.* **1985**, *31 (3)*, 449–456. DOI: https://doi.org/10.1002/aic.690310312
[19] M. Serwinski, A. Górak, *Verfahrenstechnik* **1983**, *17 (8)*, 469–473.
[20] A. Higler, R. Krishna, R. Taylor, *AIChE J.* **1999**, *45 (11)*, 2357–2370. DOI: https://doi.org/10.1002/aic.690451111
[21] A. Higler, R. Krishna, R. Taylor, *Ind. Eng. Chem. Res.* **1999**, *38 (10)*, 3988–3999. DOI: https://doi.org/10.1021/ie990261l
[22] S. Pelkonen, A. Górak, A. Ohligschläger, R. Kaesemann, *Chem. Eng. Process.* **2001**, *40 (3)*, 235–243. DOI: https://doi.org/10.1016/S0255-2701(00)00117-3

[23] S. Pelkonen, R. Kaesemann, A. Górak, *Ind. Eng. Chem. Res.* **1997**, *36 (12)*, 5392–5398. DOI: https://doi.org/10.1021/ie970333d
[24] D. R. Cruise, *J. Chem. Educ.* **1966**, *43 (1)*, 30–33.
[25] G. Ronge, *Überprüfung unterschiedlicher Modelle für den Stoffaustausch bei der Rektifikation in Packungskolonnen*, Fortschrittberichte VDI, Vol. 390, VDI Verlag, Düsseldorf **1995**.
[26] R. Baur, R. Krishna, R. Taylor, *AIChE J.* **2005**, *51 (3)*, 854–866. DOI: https://doi.org/10.1002/aic.10328
[27] R. Taylor, R. Baur, R. Krishna, *AIChE J.* **2004**, *50 (12)*, 3134–3148. DOI: https://doi.org/10.1002/aic.10278
[28] D. B. van Dongen, M. F. Doherty, *Ind. Eng. Chem. Fundam.* **1985**, *24 (4)*, 454–463. DOI: https://doi.org/10.1021/i100020a010
[29] O. M. Wahnschafft, J. W. Koehler, E. Blass, A. W. Westerberg, *Ind. Eng. Chem. Res.* **1992**, *31 (10)*, 2345–2362. DOI: https://doi.org/10.1021/ie00010a014
[30] A. Vogelpohl, *Chem. Ing. Tech.* **1964**, *36 (10)*, 1033–1045. DOI: https://doi.org/10.1002/cite.330361009
[31] S. Agarwal, R. Taylor, *Ind. Eng. Chem. Res.* **1994**, *33 (11)*, 2631–2636. DOI: https://doi.org/10.1021/ie00035a014
[32] F. J. L. Castillo, G. P. Towler, *Chem. Eng. Sci.* **1998**, *53 (5)*, 963–976. DOI: https://doi.org/10.1016/S0009-2509(97)00418-1
[33] A. Górak, A. Vogelpohl, *Sep. Sci. Technol.* **1985**, *20 (1)*, 33–61. DOI: https://doi.org/10.1080/01496398508060674
[34] H. Mori, R. Ibuki, K. Taguchi, K. Futamura, Ž. Olujić, *Chem. Eng. Sci.* **2006**, *61 (6)*, 1760–1766. DOI: https://doi.org/10.1016/j.ces.2005.10.027
[35] S. Pelkonen, M. in der Weide, A. Górak, *Chem. Ing. Tech.* **1996**, *68 (8)*, 940–943. DOI: https://doi.org/10.1002/cite.330680808
[36] P. A. M. Springer, R. Krishna, *Int. Commun. Heat Mass Transfer* **2001**, *28 (3)*, 347–356. DOI: https://doi.org/10.1016/S0735-1933(01)00240-8
[37] L. J. Krolikowski, *AIChE J.* **2006**, *52 (2)*, 532–544. DOI: https://doi.org/10.1002/aic.10663
[38] P. A. M. Springer, R. Baur, R. Krishna, *Sep. Purif. Technol.* **2002**, *29 (1)*, 1–13. DOI: https://doi.org/10.1016/S1383-5866(01)00157-5
[39] P. A. M. Springer, R. Baur, R. Krishna, *Chem. Eng. Res. Des.* **2003**, *81 (4)*, 413–426. DOI: https://doi.org/10.1205/026387603765173682
[40] P. A. M. Springer, B. Buttinger, R. Baur, R. Krishna, *Ind. Eng. Chem. Res.* **2002**, *41 (6)*, 1621–1631. DOI: https://doi.org/10.1021/ie010388m
[41] P. A. M. Springer, S. van der Molen, R. Baur, R. Krishna, *Chem. Eng. Res. Des.* **2002**, *80 (6)*, 654–666. DOI: https://doi.org/10.1205/026387602760312863
[42] P. A. M. Springer, S. van der Molen, R. Krishna, *Comput. Chem. Eng.* **2002**, *26 (9)*, 1265–1279. DOI: https://doi.org/10.1016/S0098-1354(02)00039-X
[43] G. Q. Wang, X. G. Yuan, K. T. Yu, *Ind. Eng. Chem. Res.* **2005**, *44 (23)*, 8715–8729. DOI: https://doi.org/10.1021/ie050017w
[44] C. R. Wilke, C. Y. Lee, *Ind. Eng. Chem.* **1955**, *47 (6)*, 1253–1257. DOI: https://doi.org/10.1021/ie50546a056
[45] E. N. Fuller, P. D. Schettler, J. C. Giddings, *Ind. Eng. Chem.* **1966**, *58 (5)*, 18–27. DOI: https://doi.org/10.1021/ie50677a007
[46] Z. T. Fidkowski, M. F. Doherty, M. F. Malone, *AIChE J.* **1993**, *39 (8)*, 1303–1321. DOI: https://doi.org/10.1002/aic.690390806
[47] J. G. Stichlmair, J.-R. Herguijuela, *AIChE J.* **1992**, *38 (10)*, 1523–1535. DOI: https://doi.org/10.1002/aic.690381005
[48] S. Widagdo, W. D. Seider, *AIChE J.* **1996**, *42 (1)*, 96–130. DOI: https://doi.org/10.1002/aic.690420110
[49] J. Stichlmair, *Chem. Ing. Tech.* **1988**, *60 (10)*, 747–754. DOI: https://doi.org/10.1002/cite.330601005
[50] A. Vogelpohl, *Chem. Eng. Technol.* **2002**, *25 (9)*, 869–872. DOI: https://doi.org/10.1002/1521-4125(20020910)25:9<869:AID-CEAT869>3.0.CO;2-9

